

Growth kinetics and crystal structure of semiconductor nanowiresV. G. Dubrovskii,^{1,2,*} N. V. Sibirev,¹ J. C. Harmand,³ and F. Glas³¹*St.-Petersburg Physics and Technology Centre for Research and Education, Russian Academy of Sciences, Khlopina 8/3, 195220 St.-Petersburg, Russia*²*Ioffe Physical Technical Institute, Russian Academy of Sciences, Politekhnicheskaya 26, 194021 St.-Petersburg, Russia*³*CNRS-LPN, Route de Nozay, 91460 Marcoussis, France*

(Received 11 August 2008; published 1 December 2008)

Theoretical model for the growth of semiconductor nanowires is developed, which enables one to determine the growth conditions under which the formation of nanowires is possible. General expression for the nanowire growth rate as function of its radius and the growth conditions is obtained and analyzed. The model also describes the transformation from cubic to hexagonal crystal phase of nanowires. It is shown that the observed crystal structure is controlled mainly by the growth kinetics. Structural diagrams and probabilities of cubic and hexagonal phase formation are calculated as functions of supersaturation and nanowire radius within the plausible range of material parameters. Numerical estimates for the domains of phase mixing and phase purity are presented and analyzed.

DOI: [10.1103/PhysRevB.78.235301](https://doi.org/10.1103/PhysRevB.78.235301)

PACS number(s): 81.10.Aj, 68.70.+w

I. INTRODUCTION

A rapidly growing interest in self-standing semiconductor nanowires (NWs) ranges from the fundamental physics of their growth,^{1–3} transport,⁴ and optical⁵ phenomena to many promising applications in nanoelectronics,^{6,7} nanophotonics,⁸ and nanosensing.⁹ Highly anisotropic Si crystals with micrometric radii were first fabricated by the so-called vapor-liquid-solid (VLS) mechanism in 1964.¹⁰ Using modern epitaxy techniques, NWs with radii of the order of ten nanometers and lengths up to several tens of micrometers can be obtained. Usually, NWs are grown on the surfaces activated by metal (e.g., Au) seed drops. NW materials include Si,^{2,9} Ge,⁴ III-V,^{1,3,5–7} and II-VI (Refs. 8 and 11) compounds.

For fundamental studies as well as applications, it is paramount to investigate the NW growth properties as they (in largest measure) determine the morphology and crystal structure of NW ensembles. Experiments show that NWs can be grown only within a restricted domain of deposition conditions.^{1,12–15} Taking the example of the Au-assisted molecular-beam epitaxy (MBE), the temperature window for NW formation extends from 400 to 620 °C for GaAs (Ref. 12) and only from 380 to 430 °C for InAs.¹³ The upper temperature limit cannot be explained entirely by the re-evaporation, which remains relatively small at such conditions.¹⁶ The lower limit cannot be attributed only to the solidification of catalyst particle. In particular, the temperature domain of epitaxial InAs NW is below the melting point of bulk Au-In alloy (454 °C), so the growth should at least partly proceed via the vapor-solid-solid (VSS) mechanism.¹⁴ Understanding of these growth limitations, therefore, requires a more detailed analysis of kinetic growth processes, among which nucleation^{17–19} and surface diffusion^{1–3,12,13,15,20} are generally recognized to play an important role. It is also vital to understand the role of Gibbs-Thomson (GT) effect,^{1,17} influencing the domains of NW formation, particularly for small radii.

One of the most surprising features of NWs is that their crystal structure may differ from the bulk form. Recent stud-

ies demonstrate that III-V NWs of cubic (CUB) zinc-blende materials often adopt hexagonal (HEX) wurtzite structure. This phenomenon has been reported for most zinc-blende compounds and epitaxy techniques both for Au assisted^{13,19,21} and selective area²² growth. Recently, HEX diamond lattice was experimentally observed in Si NWs.²³ In many cases, the structure of NWs is not stable and exhibits a spontaneous switching between different phases, creating rotational twins and stacking faults.¹⁴ This clearly impedes material properties, so the control over the phase purity is now considered as one of the main challenges in NW technology. The prevalence of the HEX phase might be due to a large contribution of sidewall facets²⁴ or the edges between the facets²⁵ into the overall formation enthalpy. The specific energies of these features must be indeed smaller in HEX phase.^{19,23–27} However, pure equilibrium considerations yield values of critical radius of CUB to HEX transition well below the experimentally observed values.^{19,25,27} The model developed in Ref. 19 demonstrates the effect of liquid supersaturation on the crystal structure and is supported by recent experimental findings.^{21,28} Since supersaturation during the NW formation is determined by the deposition process, the NW phase will also depend on the *growth kinetics*.

This work addresses two issues of NW formation discussed above. We present a theoretical model that (i) formulates general conditions under which the NW growth is possible and (ii) describes the probabilities of CUB and HEX phase formations depending on the material constants, the supersaturation, and the radius. Since the conditions of NW formation impose certain limitations on the supersaturation and NW size, influencing the crystal structure, the two issues above cannot be studied separately. In other words, we combine the criteria under which NWs *actually grow* and form in *HEX phase*. We consider the NW materials which, under bulk form, have stable CUB structure. We study the NWs growing on the (111) surface [e.g., Si NWs on the Si(111) or GaAs NWs on the GaAs(111)B substrate]. In the case of III-V materials, the V/III fluxes ratio is assumed to be fixed at group V (As) rich conditions.^{3,12,13} The following analysis will be referred to the most common case of VLS mecha-

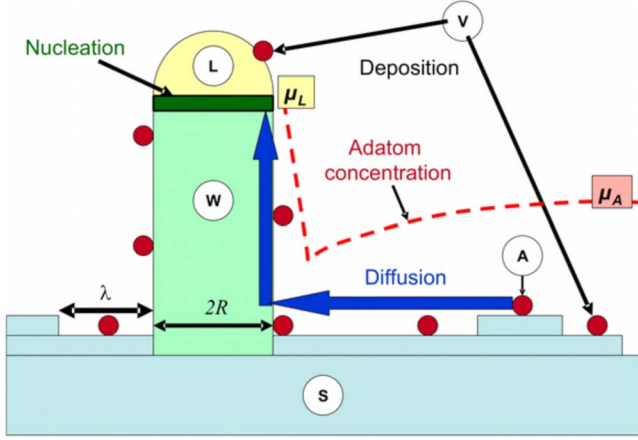


FIG. 1. (Color online) Schematics of growth model: diffusion-induced VLS growth of wire (W) from the vapor phase (V) on the cubic (111) substrate (S) through the liquid (L) in the drop and through the surface adatoms (A); the dotted line shows adatom concentration profile at $\mu_A > \mu_L$.

nism, although the conclusions drawn will also apply to VSS growth. While referring to experimental data we will consider, for concreteness, the results for the Au-assisted MBE of GaAs NWs.^{19,28}

II. MODEL

In our model we account for the following generally recognized facts. (i) The formation of NWs is strongly influenced by the GT effect of elevation of chemical potential in the drop^{1,17} and in the NW (Refs. 17, 27, and 29) with a curved surface. (ii) The growth of NWs is mediated by two-dimensional nucleation of crystal phase from a supersaturated alloy in the drop.¹⁷⁻¹⁹ (iii) The growth of Si and III-V NWs during MBE,^{2,3,12,13} chemical beam epitaxy,^{1,15} metal organic vapor pressure epitaxy,³⁰ and magnetron sputtering deposition³¹ is strongly dependent on the diffusion of adatoms from the substrate surface to the drop. (iv) NWs of CUB materials can form in HEX phase.^{13,19,21-23}

The model of NW formation via the VLS mechanism is illustrated in Fig. 1. We consider stationary growth of a prismatically or cylindrically shaped NW with constant radius R . The latter approximately equals the radius of the drop R_L so that the contact angle β is close to 90° . In view of experimental facts (iii) and (iv), we generally need to consider five phases of semiconductor material: vapor (V) with chemical potential μ_V , adatoms (A) with chemical potential μ_A , liquid (L) with chemical potential μ_L , NW (W) with chemical potential μ_W , and substrate (S) with chemical potential μ_S . The thermodynamic driving force for the growth is the difference of chemical potentials between the vapor and the substrate, $\Delta\mu_{VS} = \mu_V - \mu_S$, determined by the surface temperature T and deposition rate V (nm/s): $\Delta\mu_{VS} = k_B T \ln(V/V_0^S) = E_A + \Lambda - k_B T \ln(h\nu_A/V)$.^{32,33} Here, V_0^S is the equilibrium deposition rate at given temperature at which the deposition equalizes the desorption from the substrate surface, E_A is the activation energy of desorption, Λ is the specific condensation heat of the adatom-substrate phase transition, ν_A is the vibration fre-

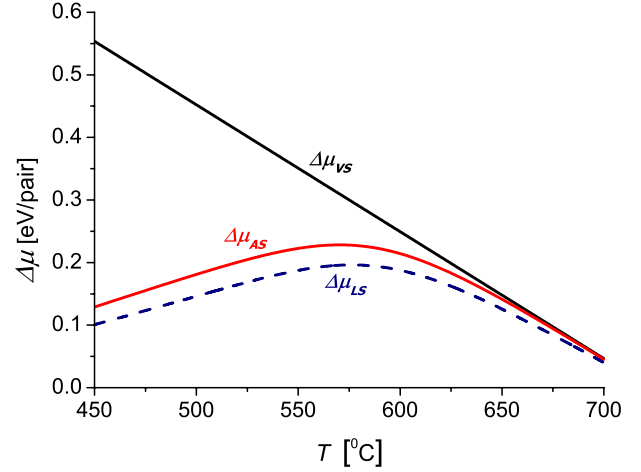


FIG. 2. (Color online) Dependences of $\Delta\mu_{VS}$ and $\Delta\mu_{AS}$ on T at fixed $V=0.6$ ML/s for the parameters of GaAs described in text. The dotted line is the liquid-solid chemical potential used in the calculations in Sec. III.

quency, h is the height of a monolayer (ML), and k_B is the Boltzmann constant. The chemical potential of adatoms far away from the NW, μ_A^∞ , is lower than μ_V due to surface nucleation. For the difference of chemical potentials between the adatoms and the substrate far away from the NW, $\Delta\mu_{AS} = \mu_A^\infty - \mu_S$, one can write

$$\Delta\mu_{AS} = \Delta\mu_{VS} - 2k_B T \ln(\lambda_0/\lambda). \quad (1)$$

Here, λ_0 is the diffusion length of adatom at the equilibrium condition between a bare substrate and the vapor phase, while λ is the effective diffusion length when the growth occurs (which implies $\lambda \leq \lambda_0$).

Typical graphs of $\Delta\mu_{VS}$ and $\Delta\mu_{AS}$ as functions of T at fixed V are presented in Fig. 2. In calculations by means of Eq. (1), we used the parameters of MBE of GaAs on the GaAs(111)B surface from atomic Ga and dimer As_2 beams (at V/III ratio=3): $E_A=1.8$ eV, $\Lambda=0.22$ eV, $\nu_A=10^{10}$ s⁻¹, and $\lambda_0=1.5$ μm for Ga atom at $T=550$ $^\circ\text{C}$. We took the Arrhenius temperature behavior of the diffusion length $\lambda_0 \propto \exp[(E_A - E_D)/2k_B T]$ with the activation energy for diffusion $E_D=0.4$ eV.³⁴ We also utilized the self-consistent model of Refs. 20 and 33 for the T and V dependences of λ_0/λ . As seen from the curves in Fig. 2, $\Delta\mu_{VS}$ decreases linearly with T and increases logarithmically with V . The behavior of $\Delta\mu_{AS}$ at low vapor supersaturation (large T and small V) matches $\Delta\mu_{VS}$ because the growth rate of the surface tends to zero and the adatoms are at the chemical potential of the vapor. At high vapor supersaturation (small T and large V), $\Delta\mu_{AS}$ is much lower than $\Delta\mu_{VS}$ because the effective diffusion length λ is limited by the surface nucleation, whose rate generally increases with decreasing T and increasing V .²⁰ As a result, the T dependence of $\Delta\mu_{AS}$ reaches the maximum at a certain temperature. In the case of GaAs MBE at $V=0.6$ ML/s the maximum is reached at approximately 570 $^\circ\text{C}$.

Our plan is to determine the conditions of NW formation by surface diffusion [fact (iii)] in the presence of GT effect [fact (i)], which is consistent with the nucleation-mediated

growth on the NW top [fact (ii)]. We will consider in detail the free enthalpy of island formation in different positions. The vapor and adatom chemical potentials are considered below as known functions of the growth conditions, similar to those presented in Fig. 2. We will then introduce different material constants for CUB and HEX NWs and investigate the relationship between the growth conditions and the crystal structure of NWs [fact (iv)].

III. DIFFUSION-INDUCED GROWTH AND GT EFFECT

The diffusion-induced growth of NWs is possible only at $\mu_A^\infty > \mu_L$ when the diffusion flux of adatoms is directed from the surface to the NW top, as shown in Fig. 1. As stated above, μ_A^∞ is the chemical potential of adatoms and $\mu_L = \mu_L^\infty + 2\Omega_L \gamma_{LV}/R_L$ is the chemical potential in the drop, which is modified by the GT effect, with γ_{LV} as the liquid-vapor surface energy, Ω_L as the elementary volume in the liquid phase, and $R_L = R/\sin \beta$ as the drop radius.^{1,17,35} Counting chemical potentials from μ_S and using Eq. (1) for $\Delta\mu_{AS}$, the condition of diffusion-induced growth can be presented in terms of liquid chemical potential at $R_L \rightarrow \infty$, $\Delta\mu_{LS}^\infty = \mu_L^\infty - \mu_S$, in the form

$$\Delta\mu_{LS}^\infty < \Delta\mu_{VS} - 2k_B T \ln\left(\frac{\lambda_0}{\lambda}\right) - \frac{2\gamma_{LV}\Omega_L \sin \beta}{R} \equiv \Delta\mu_{\max}. \quad (2)$$

This yields the upper limit for the liquid supersaturation corresponding to a positive diffusion flux to the NW top. The condition given by Eq. (2) contains two corrections to the obvious inequality $\Delta\mu_{LS} < \Delta\mu_{VS}$: one is caused by the surface nucleation and another by the curvature of drop surface.

We now show how the above condition influences the formation of NW and modifies the previously obtained results of Refs. 1, 3, 20, 36, and 37 concerning the NW growth rate, dL/dt . In a steady state, the adatom concentration on the substrate surface, denoted hereafter by n , obeys the diffusion equation

$$D\Delta n + J - \frac{n}{\tau} = 0. \quad (3)$$

Here, D is the diffusion coefficient, $J = V/\Omega_S$ is the impinging flux (Ω_S is the elementary volume in the CUB substrate phase), and τ is the effective lifetime on the substrate surface such that $\lambda = \sqrt{D\tau}$. The solution to Eq. (3), consistent with the condition $n(r) \rightarrow 0$ at $r \rightarrow \infty$ (r is the distance from the NW center in the substrate plane), is given by

$$n(r) = J\tau + CK_0(r/\lambda), \quad (4)$$

where K_0 is the modified Bessel function of the second kind. The constant C should be determined by the second boundary condition at the NW foot. Different boundary conditions lead to different expressions for the growth rate.^{1,36,37} Assuming, for simplicity, that all adatoms arriving at the NW foot are transferred to the top, we impose the condition $\Delta\mu_{AS}(r=R) = \Delta\mu_{LS} = \Delta\mu_{LS}^\infty + 2\gamma_{LV}\Omega_L \sin \beta/R$. We therefore ignore the direct impingement, the desorption, and the nucle-

ation at the sidewalls. Since the adatom gas is dilute, one can use the formula $\Delta\mu_{AS}(r) = k_B T \ln[n(r)/n_{\text{eq}}]$, where $n_{\text{eq}} = J^s \tau_0 = (V_0^s/\Omega_S)\tau_0$ is the equilibrium adatom concentration and τ_0 is the mean lifetime of an adatom on the bare substrate.³² The latter expression is consistent with Eq. (1) at $r \rightarrow \infty$ in view of $n(\infty) = J\tau$, $\tau/\tau_0 = \lambda^2/\lambda_0^2$, and $\Delta\mu_{VS} = k_B T \ln(V/V_0^s)$. We therefore get

$$n(R) = n_{\text{eq}} \exp\left(\frac{\Delta\mu_{LS}^\infty}{k_B T} + \frac{R_{\text{GT}}}{R}\right), \quad (5)$$

where $R_{\text{GT}} = \frac{2\gamma_{LV}\Omega_L \sin \beta}{k_B T}$ is the characteristic radius describing the GT effect in the drop. After equalizing the values of $n(R)$ from Eqs. (4) and (5), the solution for $n(r)$ is obtained as

$$\frac{n(r)}{J\tau} = 1 - \left[1 - \exp\left(\frac{\Delta\mu_{LS}^\infty - \Delta\mu_{AS}}{k_B T} + \frac{R_{\text{GT}}}{R}\right)\right] \frac{K_0(r/\lambda)}{K_0(R/\lambda)}. \quad (6)$$

The diffusion flux to the base of the NW, which in our approximation equals the flux to the top, is

$$j_{\text{diff}} = 2\pi R D \left. \frac{dn}{dr} \right|_{r=R}. \quad (7)$$

Using Eq. (6) in Eq. (7) and dividing the result by the factor $(\pi R^2/\Omega_S)$, the diffusion-induced contribution to the NW growth rate writes

$$\left(\frac{dL}{dt}\right)_{\text{diff}} = V \left[1 - \exp\left(\frac{\Delta\mu_{LS}^\infty - \Delta\mu_{AS}}{k_B T} + \frac{R_{\text{GT}}}{R}\right)\right] \frac{2\lambda K_1(R/\lambda)}{R K_0(R/\lambda)}, \quad (8)$$

where K_1 is the modified Bessel function of the second kind of first order. The sign of the bracket term in Eqs. (6) and (8) is positive when the inequality of Eq. (2) is satisfied and negative otherwise. The form of Eqs. (6) and (8) is similar to that of Refs. 1, 20, 36, and 37; however, the GT correction is different. It is also different from the conventional Givargizov-Chernov expression²⁹ since it contains the liquid-vapor surface energy rather than the solid-vapor one.

The adsorption-desorption contribution to the growth rate, caused by the direct interaction with the drop surface, in the case of MBE is determined by $(\pi R^2/\Omega_S)(dL/dt)_{A-D} = \pi R^2(J - J_{\text{des}}^L)$. This equation is written for beams that are strictly perpendicular to the surface. It can easily be modified in the case of vapor pressure epitaxy. The desorption rate from the drop increases with the curvature of its surface as $J_{\text{des}}^L = J_{\text{des}}^L \exp(R_{\text{GT}}/R)$, which is exactly equivalent to the elevation of equilibrium pressure of the vapor surrounding the drop.^{1,35} Since, by definition, $J/J_{\text{des}}^L = \exp(\Delta\mu_{VL}^\infty/k_B T)$ and $\Delta\mu_{VL}^\infty = \Delta\mu_{VS} - \Delta\mu_{LS}^\infty$, the direct flux to the drop is equal to

$$\left(\frac{dL}{dt}\right)_{A-D} = \frac{V}{\sin^2 \beta} \left[1 - \exp\left(\frac{\Delta\mu_{LS}^\infty - \Delta\mu_{VS}}{k_B T} + \frac{R_{\text{GT}}}{R}\right)\right]. \quad (9)$$

The resulting growth rate is the sum of contributions given by Eqs. (8) and (9), from which we must subtract the growth rate of nonactivated surface V_S .³ Since $1 - V_S/V$ in our model is exactly the probability of re-evaporation from the substrate, we have $1 - V_S/V = (\lambda/\lambda_0)^2$. Collecting all contribu-

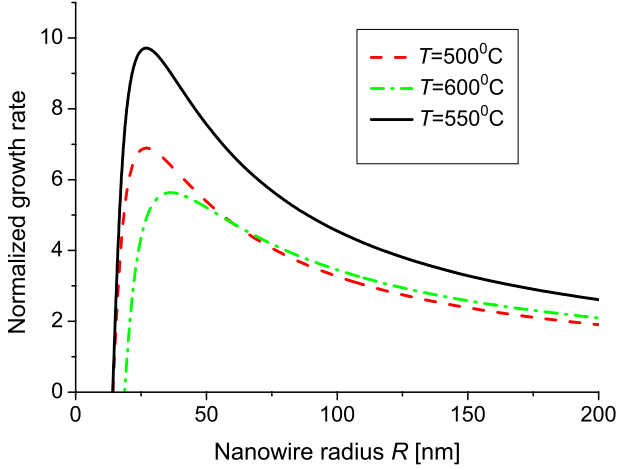


FIG. 3. (Color online) Radius dependences of normalized growth rate, $(dL/dt)/V$, at fixed $V=0.6$ ML/s for the parameters of GaAs described in text and three different temperatures $T=500$, 550, and 600 °C.

tions and using Eq. (1), the expression for the NW growth rate takes the form

$$\frac{1}{V} \left(\frac{dL}{dt} \right) = \left[1 - \exp \left(\frac{\Delta\mu_{LS}^{\infty} - \Delta\mu_{AS}}{k_B T} + \frac{R_{GT}}{R} \right) \right] \times \left[\frac{1}{\sin^2 \beta} \exp \left(\frac{\Delta\mu_{AS} - \Delta\mu_{VS}}{k_B T} \right) + \frac{2\lambda K_1(R/\lambda)}{R K_0(R/\lambda)} \right]. \quad (10)$$

Generalization of this formula that includes the adatom kinetics on the sidewalls can be done in line with the approach of Ref. 36.

The value of liquid supersaturation $\Delta\mu_{LS}^{\infty}$ in Eq. (10) remains unknown. It should be obtained from the equation of material balance in the drop.³⁸ However, the analysis of Eq. (10) enables one to draw several general conclusions concerning the NW growth kinetics. First, the NW growth rate becomes zero at minimum radius, $R_{\min} = (2\gamma_{LV}\Omega_L \sin \beta) / (\Delta\mu_{AS} - \Delta\mu_{LS}^{\infty})$, when both the adsorption-desorption and the diffusion contributions disappear. The value of R_{\min} is different from that of Refs. 1 and 17 because we take into account the GT correction in the drop and impose the condition $\Delta\mu_{AS}(r=R) = \Delta\mu_{LS}$ at the NW foot. Second, the NW growth rate as a function of its radius at fixed growth conditions is a function *with one maximum*, which agrees with the result of Ref. 1. Typical R dependences for Au-assisted MBE of GaAs NWs are shown in Fig. 3. The curves are obtained from Eq. (10) for the substrate parameters of Fig. 2 with a liquid-vapor surface energy of $\gamma_{LV} = 1$ J/m², which is between the surface energies of pure liquid Ga and Au [0.72 and 1.14 J/m² (Ref. 16)], $\Omega_L = 0.038$ nm³ per pair in the liquid phase,³⁴ $\beta = 90^\circ$ and $\Delta\mu_{LS}^{\infty}$ shown by the dotted line in Fig. 2. The growth of thin NWs is mainly determined by the GT effect, and dL/dt increases with R . The maximum of dL/dt is reached due to a *competition* between the GT effect and the adatom diffusion. The position and the value of this maximum depend on the sur-

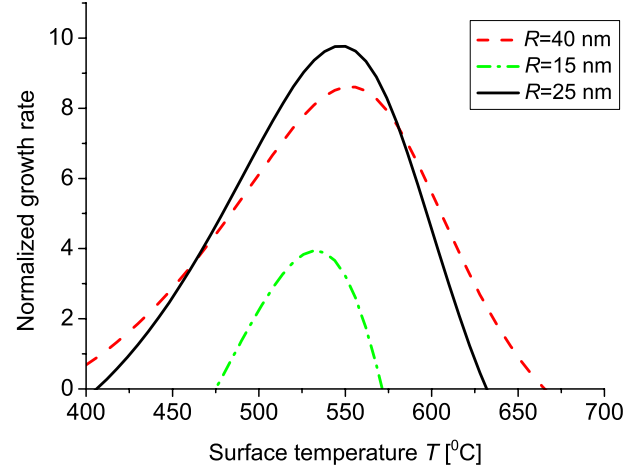


FIG. 4. (Color online) Temperature dependences of normalized growth rate for the parameters described in text and three different radii $R=15$, 25, and 40 nm.

face temperature. For larger R , the situation is reverse and dL/dt decreases in normal diffusion-induced mode.¹⁻³ Third, the T dependences of NW growth rate at fixed R , presented in Fig. 4 for the same parameters of GaAs, are also functions with one maximum, which is supported by the results of Refs. 12, 13, 15, and 20. The maximum is explained by the nonmonotonous behavior of $\Delta\mu_{AS}$, which was discussed earlier. The obtained temperature domain of NW growth with $dL/dt > 0$ is close to the experimentally observed window ranging from 400 to 620 °C for GaAs NWs.¹² The growth domain is narrower for smaller R , while the maximum growth rate is reached at intermediate R (25 nm in Fig. 4).

IV. NUCLEATION

For the analysis of nucleation at the NW top [fact (ii)], we should calculate the free enthalpy (more precisely, the minimum work³⁵) of isothermal ($T=\text{const}$) formation of a crystal island of arbitrary shape with linear size (“radius”) r , monolayer height h , area $A=c_1 r^2$, and perimeter $P=c_2 r$. This is not a simple problem because, due to the small size of the drop, the characteristics of metastable (liquid) phase are generally perturbed by the island formation. If the liquid pressure remains approximately constant during nucleation, the free enthalpy of the “drop-island” system changes due to (i) the decrease in chemical potential of $i=(Ah)/\Omega_S$ semiconductor particles from μ_L^{∞} in the liquid alloy to μ_W^{∞} in the NW; (ii) the formation of island lateral surface Ph ; and (iii) the transformation of drop surface ΔS_L due to the island formation

$$\Delta G_{\text{wire}} = -(\mu_L^{\infty} - \mu_W^{\infty})i + \Gamma_I Ph + \gamma_{LV} \Delta S_L. \quad (11)$$

The first volume term does not contain the GT correction since the latter is already taken into account in the surface energy terms. As discussed in Ref. 19, the island surface energy depends on the island position and is generally given by $\Gamma_I = (1-x)\gamma_{SL} + x\gamma_{WV}$, where γ_{SL} is the solid-liquid surface energy, γ_{WV} is the wire-vapor surface energy, and x is the fraction of the island perimeter at the triple line (TL) [see

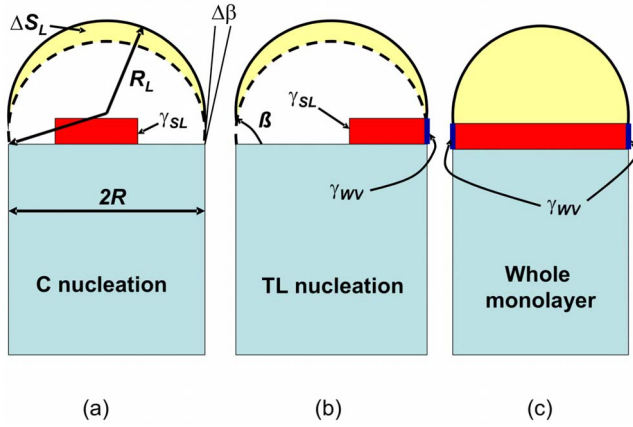


FIG. 5. (Color online) Nucleation of island in position (a) C, (b) TL, and (c) occupying the whole monolayer of NW.

Fig. 5(b)]. The values of μ_w^∞ , γ_{wv} , and Γ_l depend on the crystal structure of NW.

It should be noted that, even under the standard assumption of constant number of catalyst particles in the drop,¹⁷ the calculation of ΔS_L cannot be done in an absolute fashion. If the nucleation proceeds at a constant number of semiconductor particles, the change in liquid volume due to nucleation equals $\Delta V_L = -\Omega_L i$, the change in solid volume equals $\Delta V_W = \Omega_S i$, and the total volume change equals $\Delta V = (\Omega_S - \Omega_L) i$ (hereafter we neglect the small variations of Ω_S and h with the crystal phase). If, instead, we assume that i particles are added to the liquid during each nucleation act, then $\Delta V_L = 0$ and $\Delta V_W = \Delta V = \Omega_S i$. In Eq. (11), we also need to change μ_L^∞ to μ_V because i particles are now transferred from the vapor to the solid phase through the adatom sea and/or through the liquid. To clarify this point, we note that the nucleation at the top of sufficiently thin NWs is mononuclear, i.e., only one island succeeds in nucleation in each layer.^{17,18,39} In this mononuclear mode, the standard time scale hierarchy of condensation stages in infinitely large systems^{32,39} should be reconsidered. Namely, the duration of nucleation stage can be much shorter or comparable with the island growth stage (depending on the island size), while the latter is always much shorter than the waiting time between two successive nucleation acts. This waiting time approximately equals the growth rate of the NW ML itself. Therefore, semiconductor atoms can only be added to the drop after the formation of the island nucleus. This preserves the stationary character of NW growth with constant R (averaged over the time of growth of one ML) and identical nucleation conditions for each ML and on the other hand, shows that nucleation takes place at a constant number of particles in the “liquid-plus-island” system. In order to distinguish two possible scenarios of NW growth (from the liquid phase in the drop and from the vapor phase at a constant liquid volume), we now introduce two stages of growth.

(1) *Fast microscopic stage 1* of nucleation of each ML from the liquid phase with total volume change $\Delta V_1 = (\Omega_S - \Omega_L) i$. (2) *Slow macroscopic stage 2* of NW growth from the vapor phase with total volume change $\Delta V_2 = 2\pi R h$ (in this case $i = i_{\max} = 2\pi R h / \Omega_S$ is the number of particles in a complete ML of NW).

As will be shown later on, the growth stage strongly influences not only the nucleation kinetics but also the resulting crystal structure of NWs.

Considering the fast stage 1, we first calculate the change of surface area ΔS_L and of the drop radius ΔR_L after the formation of island with i particles in the center of the liquid-solid interface (C), so that $x=0$, as shown in Fig. 5(a). We utilize the known expressions for the volume and the surface area of a spherical cap, $V_{\text{drop}} = (\pi R^3/3)[(1 - \cos \beta)^2(2 + \cos \beta)]/\sin^3 \beta$ and $S_{\text{drop}} = [2\pi R^2(1 - \cos \beta)]/\sin^2 \beta$. At $R = \text{const}$, these quantities are functions of the contact angle β only. In the case of C nucleation, the liquid phase entirely surrounds the island; therefore, $\Delta S_L = \Delta S_{\text{drop}}$, $\Delta V_{\text{drop}} = \Delta V_1 > \Delta V_L$, and the liquid surface increases. Considering $\Delta \beta$ as a small quantity and finding it for the given volume change, after some straightforward calculations we obtain the following expressions for ΔS_L and ΔR_L :

$$\Delta S_L = \frac{2 \sin \beta}{R} (\Omega_S - \Omega_L) i;$$

$$\Delta R_L = -\frac{1}{\pi R^2} \frac{\sin^2 \beta \cos \beta}{(1 - \cos \beta)^2} (\Omega_S - \Omega_L) i. \quad (12)$$

If the island occupies the *whole monolayer* [Fig. 5(c)], the liquid is *ousted* by the solid. In this case $\Delta S_L = \Delta S_{\text{drop}}$, but $\Delta V_{\text{drop}} = \Delta V_L = -\Omega_L i_{\max}$ and the liquid surface decreases. By the same procedure, we get

$$\Delta S_L = -\sin \beta \frac{\Omega_L}{\Omega_S} 2\pi R h; \quad \Delta R_L = \frac{\sin^2 \beta \cos \beta \Omega_L}{(1 - \cos \beta)^2 \Omega_S} h. \quad (13)$$

For nucleation at the TL [Fig. 5(b)] of an island of arbitrary size, the quantity ΔS_L cannot be calculated exactly. We can, however, combine Eqs. (12) and (13) for ΔS_L at arbitrary i because TL nucleation eliminates some part of the liquid surface at the TL. This gives

$$\Delta S_L = \frac{2 \sin \beta}{R} (\Omega_S - \Omega_L) i - \sin \beta \frac{\Omega_L}{\Omega_S} x P h. \quad (14)$$

Equations (12)–(14) demonstrate that the term $\gamma_{LV} \Delta S_L$ is generally of the order of the surface energy of the island. It is also seen that ΔR_L is zero at $\beta = 90^\circ$, so that the surface area changes without changing its curvature (because R_L reaches its minimum at $\beta = 90^\circ$ at fixed R). Therefore, the Laplace pressure in the liquid $P_L = 2\gamma_{LV}/R_L$ is approximately constant before and after nucleation at $\beta \cong 90^\circ$, and the minimum work of island formation is given by Eq. (11). At large $\beta > 90^\circ$, the term $V_L \Delta P_L$ becomes comparable with other contributions in Eq. (11). This case should be considered separately because, generally, the minimum work of island formation at variable pressure is unknown and cannot be described by any thermodynamic potential.

Substitution of Eq. (14) into Eq. (11) gives the result for free enthalpy of island formation at the fast nucleation stage,

$$\Delta G_{\text{wire}}^{(1)} \equiv \Delta G_{\text{wire}} = - \left[\Delta \mu_{LS}^{\infty} - \psi - \frac{2\gamma_{LV}(\Omega_S - \Omega_L)\sin\beta}{R} \right] \frac{c_1 r^2 h}{\Omega_S} + \Gamma c_2 r h. \quad (15)$$

Here,

$$\Gamma = (1-x)\gamma_{SL} + x(\gamma_{WV} - \gamma_{LV}\sin\beta) \quad (16)$$

is the effective surface energy of the island introduced in Ref. 19. The quantity ψ is zero for CUB phase and $\psi = \psi_{\text{HEX}}$ for HEX phase, with ψ_{HEX} as the difference of bulk cohesive energies between HEX and CUB phases at zero pressure [$\psi_{\text{HEX}} = 24$ meV per pair for GaAs (Ref. 40)]. The value of γ_{WV} depends on the crystal structure of NW, the type of lateral facets [e.g., (110) or (221) plane], and is usually lower in HEX than in CUB phase.^{19,25–27} Nucleation in position C proceeds at $\Gamma = \gamma_{SL}$, with γ_{SL} as the surface energy of the solid-liquid lateral interface. Following Glas *et al.*,¹⁹ we will assume that γ_{SL} is identical for nuclei in CUB and HEX orientations because of the close atomic environments on the surface around the two types of nuclei. Equations (15) and (16) are similar to the expression of Ref. 19 for monolayer, except for the additional term $2\gamma_{LV}(\Omega_S - \Omega_L)i/R_L$, which is caused by the change in elementary volume after solidification. This contribution can be of either sign and cancels only in the unlikely case where $\Omega_S = \Omega_L$.

If we consider the long stage of formation of a full NW slice from vapor, reiterative building of monolayers at constant liquid volume is described by

$$\Delta G_{\text{wire}}^{(2)} = - [\Delta \mu_{VS} - \psi] \frac{\pi R^2 h}{\Omega_S} + 2\gamma_{WV}\pi R h. \quad (17)$$

This equation at $\psi=0$ is exactly identical to the Givargizov-Chernov correction of chemical potential of the NW, $\Delta \mu_{VS} = \Delta \mu_{VS}^{\infty} - 2\gamma_{WV}\Omega_S/R$, while considering the growth of whisker from a vapor phase through the liquid.²⁹ Such an expression has been used in many other works, in particular, in Ref. 27 for modeling of *growth thermodynamics* of NWs and polytypism of zinc-blende III-V NWs. It should be noted, however, that if the island is first nucleated in, say, HEX orientation and fills the complete ML in HEX, it would be very difficult to rotate the whole ML by 60° to transform it to CUB, although the free enthalpy defined by Eq. (17) might be lower in CUB orientation. We therefore conclude that the crystal structure of NWs is controlled by the *growth kinetics* rather than by thermodynamics, as already suggested by Johansson *et al.*⁴¹ and demonstrated by Glas *et al.*¹⁹

With this determination made, we consider hereafter the change in free enthalpy during the fast microscopic stage given by Eqs. (15) and (16). To compare the growth rates of the NW and of the nonactivated surface, we write the expression for the free enthalpy of island formation on the substrate surface from the adatoms with supersaturation $\Delta \mu_{AS}$ in the form

$$\Delta G_{\text{surface}} = - \Delta \mu_{AS} c_1 \frac{hr^2}{\Omega_S} + \gamma_{SV} c_2 hr. \quad (18)$$

The surface energy term now contains the substrate-vapor

surface energy because the surface islands always adopt the crystal phase of the substrate. Maximizing Eqs. (15) and (18) in r , one obtains the expressions for the nucleation barriers ΔG^* at the NW top and on the surface,

$$\Delta G_{\text{wire}}^* = \frac{c_2^2}{4c_1} \frac{\Gamma^2 h \Omega_S}{[\Delta \mu_{LS}^{\infty} - \psi - 2\gamma_{LV}(\Omega_S - \Omega_L)\sin\beta/R]},$$

$$\Delta G_{\text{surface}}^* = \frac{c_2^2}{4c_1} \frac{\gamma_{SV}^2 h \Omega_S}{\Delta \mu_{AS}^{\infty}}. \quad (19)$$

The critical size at the NW top is given by $r_{\text{wire}}^* = (2/c_2 h \Gamma) \Delta G_{\text{wire}}^*$. Obviously, the NW can be formed only if its growth rate, dL/dt , is larger than the vertical growth rate of the surface, dH_S/dt . The NW growth rate in the mononuclear mode is given by $dL/dt \propto (1/\tau_L)(R/l_0)^2 \exp(-\Delta G_{\text{wire}}^*/k_B T)$, where τ_L is the characteristic time of island growth from the liquid and l_0 is the lattice spacing.¹⁷ The surface always grows in the polynuclear mode when many islands arise and coalesce in one layer. The vertical growth rate in this case is written as $dH_S/dt \propto (1/\tau_A) \exp(-\Delta G_{\text{surface}}^*/3k_B T)$, where τ_A is the characteristic time of island growth from the adatoms.¹⁷ The factor 1/3 in the exponent of the surface growth rate accounts for the transition from mononuclear to polynuclear mode.¹⁸ Assuming that τ_L and τ_A are of the same order and that $\ln(R/l_0)$ is not too large, we keep only the leading exponential dependence of the growth rate on the nucleation barrier, neglecting all pre-exponential terms. From these considerations, the second condition of NW formation is $\Delta G_{\text{wire}}^* < \Delta G_{\text{surface}}^*/3$. Using Eq. (19) and the previously obtained condition for diffusion-induced growth, we obtain the following range of liquid supersaturations $\Delta \mu_{LS}^{\infty}$:

$$\Delta \mu_{\text{min}} \equiv 3 \left(\frac{\Gamma}{\gamma_{SV}} \right)^2 \Delta \mu_{AS} + \frac{2\gamma_{LV}(\Omega_S - \Omega_L)\sin\beta}{R} + \psi < \Delta \mu_{LS}^{\infty} < \Delta \mu_{AS} - 2 \sin\beta \frac{\gamma_{LV}\Omega_L}{R} \equiv \Delta \mu_{\text{max}}. \quad (20)$$

The lower limit $\Delta \mu_{\text{min}}$ is imposed by the nucleation probability, and the upper limit $\Delta \mu_{\text{max}}$ corresponds to a positive diffusion flux to the NW top. Growth criterion (20) can be satisfied only when $\Gamma/\gamma_{SV} < 1/\sqrt{3}$, which imposes the upper limit on the island surface energy Γ , which is consistent with the analysis of Ref. 17. The value of $\Delta \mu_{\text{min}}$ depends on the growth conditions through $\Delta \mu_{AS}^{\infty}$ and on the crystal phase through γ_{WV} and ψ , while $\Delta \mu_{\text{max}}$ is phase independent and is determined by the growth kinetics.

Using Eq. (1) for $\Delta \mu_{AS}$, Eq. (20) provides the lower limit for the vapor chemical potential, below which the NWs cannot be grown,

$$\Delta \mu_{VS} > \frac{\psi + 2\gamma_{LV}\Omega_S \sin\beta/R}{1 - 3(\Gamma/\gamma_{SV})^2} + 2k_B T \ln(\lambda_0/\lambda). \quad (21)$$

Generally, the vapor supersaturation should be high enough to overcome the Gibbs-Thomson effect, to ensure that the NW growth rate is larger than that of the surface, and to

TABLE I. Characteristic radius R_0 in different semiconductor NWs.

Material	Elementary volume Ω_S (nm ³)	Lateral facets	Lateral surface energy γ_{CUB} (J/m ²)	Difference of cohesive energies ψ_{HEX} (meV)	Characteristic radius R_0 (nm)
AlSb	0.0567	(110)	1.3	18.6	24
GaSb	0.0567	(110)	1.1	19.4	20
InSb	0.068	(110)	0.75	16	20
AlAs	0.0451	(110)	1.8	11.3	45
GaAs	0.0451	(110)	1.5	24	17
InAs	0.0567	(110)	1	10.3	33
AlP	0.0398	(110)	2.4	7.1	83
GaP	0.040	(110)	2	18.3	27
InP	0.0506	(110)	1.3	6.8	60
Si	0.0200	(110)	1.43–1.7	10–11.7	15–21
Si	0.0200	(211)	1.31	10–11.7	14–16

onset the CUB to HEX transformation in the case of HEX NWs.

V. CRYSTAL STRUCTURE

We now proceed to studying the crystal structure of NWs within the above-determined growth domains. For the following, it is convenient to introduce normalized differences of chemical potential with the solid for the liquid phase, $f = \Delta\mu_{LS}^\infty / \psi_{\text{HEX}}$, and for the adatoms, $a = \Delta\mu_{AS} / \psi_{\text{HEX}}$, and the radius $\rho \equiv R/R_0$ measured in units of the characteristic radius $R_0 = \gamma_{\text{CUB}}\Omega_S / \psi_{\text{HEX}}$, where $\gamma_{\text{CUB}} = \gamma_{\text{SV}}$ is the solid-vapor surface energy in CUB phase. Numerical estimates of R_0 for Si and binary III-V compounds are summarized in Table I. We used the data of Ref. 40 for ψ_{HEX} and the data of Refs. 34, 42, and 43 for γ_{CUB} of different facets. The values of ψ_{HEX} and Ω_S are given per atom for Si and per III-V pair for compounds. The data of Table I give the characteristic scales of CUB to HEX phase transformation in different semiconductors. At fixed drop radius, materials with larger R_0 should adopt HEX phase *more often* than the others.

Using the above definitions, Eq. (19) yields the following expressions for the normalized nucleation barriers in CUB and HEX NWs:

$$g_{\text{CUB}} \equiv \frac{\Delta G_{\text{CUB}}^*}{k_B T} = Q \frac{\varepsilon^2}{f - (\omega - 1)\delta/\rho};$$

$$g_{\text{HEX}} \equiv \frac{\Delta G_{\text{HEX}}^*}{k_B T} = Q \frac{(\varepsilon\eta)^2}{f - (\omega - 1)\delta/\rho - 1}. \quad (22)$$

The corresponding expressions for critical radii are

$$\rho_{\text{CUB}}^* = \frac{c_2}{4\sqrt{3}c_1} \frac{\varepsilon}{[f - (\omega - 1)\delta/\rho]};$$

$$\rho_{\text{HEX}}^* = \frac{c_2}{4\sqrt{3}c_1} \frac{\varepsilon\eta}{[f - (\omega - 1)\delta/\rho - 1]}. \quad (23)$$

The parameter $Q = (c_2^2/24c_1)(\gamma_{\text{CUB}}R_0h/k_B T)$ in Eq. (22) is determined by the island shape, the surface energy in CUB phase, and the temperature. The other coefficients are defined as follows: $\varepsilon \equiv \sqrt{3}\Gamma_{\text{CUB}}/\gamma_{\text{CUB}}$; $\eta \equiv \Gamma_{\text{HEX}}/\Gamma_{\text{CUB}}$; $\delta \equiv 2\gamma_{\text{LV}}\Omega_L/\gamma_{\text{CUB}}\Omega_S$; and $\omega = \Omega_S/\Omega_L$. Here, γ_{HEX} is the lateral surface energy of HEX NW, Γ_{CUB} is the effective surface energy of nucleus in CUB orientation, and Γ_{HEX} is the corresponding value in HEX orientation. We saw earlier that a necessary condition for NW formation is $\varepsilon < 1$. The coefficient η depends on the nucleus position. It is equal to one in position C and becomes lower than one for nucleation at the TL. The condition $g_{\text{CUB}}(f_{\text{CR}}) = g_{\text{HEX}}(f_{\text{CR}})$ determines the critical chemical potential f_{CR} , separating the domains of prevalent CUB and HEX phase formations. Using Eqs. (20) and (22), the characteristic chemical potentials take the form

$$f_{\text{min}}^{\text{CUB}} = a\varepsilon^2 + \frac{(\omega - 1)\delta}{\rho};$$

$$f_{\text{min}}^{\text{HEX}} = 1 + a(\eta\varepsilon)^2 + \frac{(\omega - 1)\delta}{\rho};$$

$$f_{\text{CR}} = \frac{1}{1 - \eta^2} + \frac{(\omega - 1)\delta}{\rho};$$

$$f_{\text{max}} = a - \frac{\delta}{\rho}. \quad (24)$$

It is seen that the Gibbs-Thomson correction for the drop curvature $-\delta/\rho$ is identical in all equations in Eq. (24), and therefore, does not affect the crystal structure. The expression for f_{CR} is useful only in the case of TL nucleation at $\eta_{\text{TL}} < 1$, which is consistent with the results of Ref. 19.

Below we adopt Eq. (16) for the surface energies of the island: $\Gamma_{\text{CUB}} = (1-x)\gamma_{\text{SL}} + x(\gamma_{\text{CUB}} - \gamma_{\text{LV}} \sin \beta)$; $\Gamma_{\text{HEX}} = (1-x)\gamma_{\text{SL}} + x(\tau\gamma_{\text{CUB}} - \gamma_{\text{LV}} \sin \beta)$, where

$$\tau = \gamma_{\text{HEX}}/\gamma_{\text{CUB}} \quad (25)$$

is the ratio of lateral surface energies of HEX and CUB NWs in contact with the vapor. As already shown in Ref. 19, CUB to HEX structural transformation *can only be observed at* $\tau < 1$. Different models for τ regards for the effects of surface dangling bonds on the lateral facets,^{24,27} the edges separating the facets,^{25,26} and the sawtooth faceting of lateral surface of CUB NWs.^{19,44} The value $\tau=0.75$ is obtained from a simple count of surface dangling bonds on the lateral facets (4/3 bonds per layer in CUB phase and 1 bond per layer in HEX phase) and pertains only to particular facets.²⁷ Since τ is generally unknown, we investigate the structural diagrams within the plausible range of τ values between 0.75 and 0.975. While the value of solid-liquid surface energy γ_{SL} is also unknown, it can be (in principle) estimated from Young's equation for the drop seated on the lateral surface of CUB crystal, $\gamma_{CUB} = \gamma_{SL} + \gamma_{LV} \cos \varphi$, by measuring the contact angle φ . Ignoring, in a first approximation, possible variations of the contact angle of the drop β with the crystal phase, we arrive at the following expressions for coefficients ε and τ in the case of C and TL nucleations:

$$\varepsilon_C = \sqrt{3} \left(1 - \frac{\gamma_{LV} \cos \varphi}{\gamma_{CUB}} \right); \quad \eta_C = 1 \quad (26)$$

$$\varepsilon_{TL} \cong \varepsilon_C - \sqrt{3} x \frac{\gamma_{LV}}{\gamma_{CUB}} (\sin \beta - \cos \varphi);$$

$$\eta_{TL} \cong \frac{\varepsilon_{TL} - \sqrt{3} x (1 - \tau)}{\varepsilon_{TL}}. \quad (27)$$

According to the second Eq. (27), coefficient η_{TL} depends on τ .

To further estimate the typical values of model parameters, we again consider the Au-assisted MBE of GaAs NWs on the GaAs(111)B surface. We use the values of $\gamma_{CUB} = 1.5$ J/m² and $\gamma_{LV} = 1$ J/m². At $\Omega_S = 0.0451$ nm³ per GaAs pair in the crystal and $\Omega_L = 0.038$ nm³ in the liquid,³⁴ the coefficient δ amounts to 1.12 and the coefficient ω to 1.19. We choose the constant value of contact angle of the drop at $\beta = 100^\circ$, which is within the experimentally observed range after growth ($90^\circ < \beta < 125^\circ$) (Ref. 19) and on the other hand, consistent with the assumption of Sec. V of $P_L \cong \text{const}$. In view of Eq. (26), the NW growth condition $\varepsilon_C < 1$ at $\gamma_{LV}/\gamma_{CUB} = 2/3$ imposes the limits on the angle φ , which must lie between 0° and 50° . We use the mean value from this growth domain, $\varphi = 25^\circ$, relating to $\gamma_{SL} = 0.594$ J/m² and $\varepsilon_C = 0.686$. As in Ref. 19, we specify the shape of the nucleus as an equilateral triangle with sides r , where one of them is at the TL ($x = 1/3$, $c_1 = \sqrt{3}/4$, and $c_2 = 3$). This readily gives $\varepsilon_{TL} = 0.656$. The values of η_{TL} at different τ are then calculated by means of the second equation in Eq. (27). With $\psi_{HEX} = 24$ meV, we obtain a characteristic radius R_0 at approximately 17 nm. The parameter Q in Eq. (22) is equal to 1294 at $T = 560^\circ\text{C}$ (with $h = 0.325$ nm). Finally, from Fig. 2 at $T = 560^\circ\text{C}$ and $V = 0.6$ ML/s, we obtain the maximum value of $\Delta\mu_{AS}^\infty$ at 230 meV, relating to $a_{\max} = 9.6$.

Analysis of Eq. (24) shows that if nucleation takes place in position C ($\eta_C = 1$), f_{\min}^{CUB} is always smaller than f_{\min}^{HEX} . The

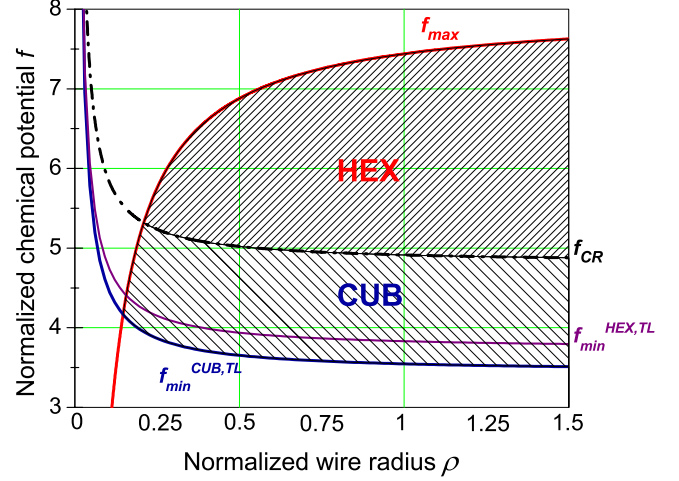


FIG. 6. (Color online) Structural phase diagrams in the case of TL nucleation at $a=8$ and $\tau=0.875$. Shaded domains, separated by the curve $f_{CR}(\rho)$, correspond to the prevalence of CUB or HEX phase.

islands will therefore tend to adopt the CUB orientation. However, for our parameters TL nucleation is *favorable* for both CUB and HEX islands, and we need to compare $f_{\min}^{\text{CUB,TL}}$, f_{CR} , and f_{\max} . Structural phase diagrams in (ρ, f) plane, obtained from Eqs. (24)–(27) at $a=8$ and $\tau=0.875$, are presented in Fig. 6. Generally, CUB phase should be prevalent between the curves $f_{\min}^{\text{CUB,TL}}(\rho)$ and $f_{CR}(\rho)$, and HEX phase dominates between the curves $f_{CR}(\rho)$ and $f_{\max}(\rho)$. This confirms the importance of supersaturation: at given ρ , CUB phase is formed at *low* and HEX phase at *high* liquid supersaturations.¹⁹ Combination of kinetic and structural considerations allows us to find the conditions of phase purity. Obviously, CUB phase should never be observed at $f_{CR}(\rho) < f_{\min}^{\text{CUB}}(\rho)$, implying $\eta_{TL} < \sqrt{1 - 1/(a\varepsilon_{TL})^2}$. For our parameters, the latter inequality relates to $\tau < 0.82$. The HEX phase could not form when $f_{CR}(\rho) > f_{\max}(\rho)$. At $\rho \gg 1$ this is reduced to $\eta_{TL} > \sqrt{1 - 1/a}$, corresponding to $\tau > 0.93$.

Calculation of probabilities of different phases is more informative for the analysis of structural stability and for the comparison with experimental data for several reasons. First, it allows for all possible growth mechanisms and describes mixing of different phases in a NW ensemble. Second, probabilistic approach accounts for the energetic barriers for the phase onset. Third, it regards for fluctuations, which become important whenever the phases are separated by the energy gap compared to or much smaller than $k_B T$. Probabilities of formation of CUB and HEX phases hereafter are defined as

$$P_{\text{CUB}} = P_{\text{CUB,C}} + P_{\text{CUB,TL}}; \quad P_{\text{HEX}} = P_{\text{HEX,C}} + P_{\text{HEX,TL}} \quad (28)$$

with $p_k = I_k / \sum_{k=1}^4 I_k$ as the normalized probabilities of “growth scenarios” $k = (\text{CUB,C})$, (CUB,TL) , (HEX,C) , and (HEX,TL) . Growth rates I_k are proportional to $\exp(-g_k)$, where g_k are the nucleation barriers in the four possible configurations given by Eq. (22) with different coefficients η and ε . Additionally, we account for the finite sizes of the top facet and the critical nuclei. Indeed, the nucleation in position C is

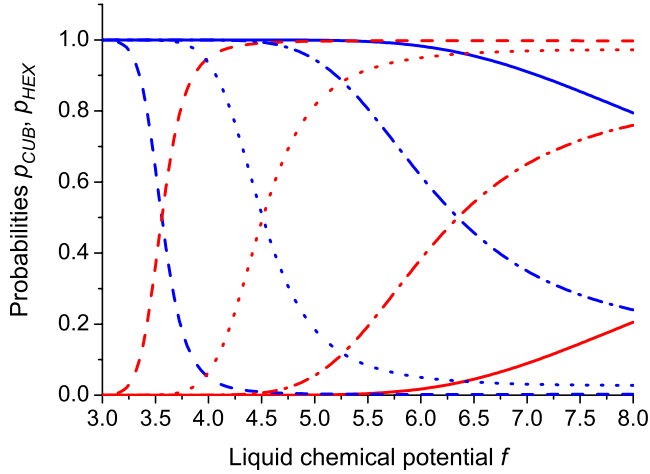


FIG. 7. (Color online) Probabilities of CUB (decreasing blue curves) and HEX (increasing red curves) phase formations as functions of f at fixed radius $\rho=1.14$; $\tau=0.95$ —solid lines, $\tau=0.91$ —dash-dotted lines, $\tau=0.875$ —dotted lines and $\tau=0.83$ —dashed lines.

possible on the whole facet without the external ring of critical radius, while the nucleation in position TL is possible only within this ring. If the critical size is larger than the facet radius, the nucleation is impossible. We therefore opt for the following expressions for I_C and I_{TL} :

$$I_C = \rho^2 \exp(-g_C) \Theta(k_C \rho - \rho_C^*);$$

$$I_{TL} = (2\rho\rho_{TL}^* - \rho_{TL}^{*2}) \exp(-g_{TL}) \Theta(k_{TL}\rho - \rho_{TL}^*). \quad (29)$$

Here, the step function $\Theta(x)=1$ at $x>0$ and $\Theta(x)=0$ at $x<0$; k_C and k_{TL} are the geometrical coefficients such that $k_C\rho$ and $k_{TL}\rho$ are the maximum size of nuclei on the facet of size ρ in C and TL positions. From simple geometrical considerations, for the NW cross section having the shape of regular hexagon with side ρ and the triangle island, we have $k_C=3/2$ and $k_{TL}=1$. Since the growth domains, determined by Eq. (24), depend on the configuration k , the nucleation rates I_k should be calculated within the k th domain and put to zero outside the domain.

In Fig. 7, we present the probabilities of CUB and HEX phase formations obtained from Eqs. (28) and (29) for the above parameters. The probabilities are plotted as functions of liquid supersaturation at fixed $\rho=1.14$, relating to $R=20$ nm in the case of GaAs NWs, and different τ . Calculations show that NWs adopt the CUB phase in the whole growth domain with nearly 100% probability at $\tau>0.97$. The curves at $\tau=0.95$ show the onset of HEX phase only at very high f with $\sim 20\%$ probability. The curves at $\tau=0.91$ and 0.875 demonstrate phase mixing at intermediate values of supersaturations with 50% mixing reached at $f=6.4$ for $\tau=0.91$ and $f=4.5$ at $\tau=0.875$. In these regions, the observation of a spontaneous switching between the phases, rotational twin layers, and stacking faults is most likely. Lower supersaturations correspond to the pure CUB phase, and higher supersaturations correspond to the pure HEX phase. At $\tau=0.83$, CUB phase is observed at very low supersatura-

tions ($f<3.5$), while the HEX structure is prevalent in the rest of the growth domain. The dominant kinetic process is TL nucleation of islands in HEX orientation. It should be noted that due to the assumption of mononuclear growth, the model in its present form is not directly applicable to very thick wires. The reduction in boundary effect on the TL nucleation will lead to the formation of CUB phase at $\rho \rightarrow \infty$, as it should be the case during the liquid phase epitaxy of two-dimensional layers.

VI. CONCLUSIONS AND OUTLOOK

To conclude, we have developed a model of NW growth, which is capable of describing the NW formation domains and the crystal phase. It has been demonstrated that the diffusion-induced growth of NWs is strongly influenced by the GT effect in the drop. A general expression for the NW growth rate has been obtained and analyzed. We have considered the nucleation in positions C and TL and derived the expression for free enthalpy of island formation, accounting for the change in surface area of liquid-vapor interface. Two stages of NW growth have been analyzed, and it has been shown that the growth rate and the crystal structure should be controlled by the fast nucleation stage rather than by the growth thermodynamics. We have formulated two general conditions of NW formation: the liquid supersaturation should be low enough to enable the diffusion of adatoms from the substrate and high enough to ensure that the NW growth rate is actually larger than that of the nonactivated surface. We then developed a model of NW phase selection, which is applicable to all NW materials with stable CUB phase under the bulk form. Furthermore, the results obtained can be used for the analysis of structural transformations in nanostructures of other types. We have presented the structural diagrams and calculated the probabilities of CUB and HEX phase formations depending on the liquid supersaturation and the material constants. It has been shown that the formation of the HEX phase requires sufficient gain in the lateral surface energy ($>3\%$). Calculations of probabilities of CUB and HEX phase formations provide the ranges of deposition conditions with nearly 100% pure structure. Therefore, the control over the phase purity of NWs by means of careful tuning of growth parameters must be possible. We now plan to calculate the liquid supersaturation by applying the equation of material balance in the drop, which would extend the present approach to modeling the dynamics of structural transformation in NWs. We intend to investigate in more detail the ways of controlling the crystal structure of Si and III-V NWs. In particular, the results obtained above can be interpreted in two ways: (1) probability to observe homogeneous NW in a given phase over the ensemble of NWs and (2) probability to observe a given proportion of the two phases within a single NW. We believe that the first interpretation is directly applicable and the second can be considered only qualitatively. We utilized the surface and cohesive energies of fully formed NWs and did not account for the influence of the structure of preceding layers on the formation of the upper ones. We plan to modify the present model to include these effects.

ACKNOWLEDGMENTS

This work was partially supported by the Russian Federal Agency for Science and Innovation (Contract No. 02.513.11.3042), the SANDIE Network of Excellence of the

European Commission (Contract No. NMP4-CT-2004-500101), and the different grants of the Russian Academy of Sciences and the Russian Foundation for Basic Research. We thank R. A. Suris and G. E. Cirlin for interesting discussions.

*Corresponding author. dubrovskii@mail.ioffe.ru

- ¹L. E. Fröberg, W. Seifert, and J. Johansson, *Phys. Rev. B* **76**, 153401 (2007).
- ²L. Schubert, P. Werner, N. D. Zakharov, G. Gerth, F. M. Kolb, L. Long, U. Gösele, and T. Y. Tan, *Appl. Phys. Lett.* **84**, 4968 (2004).
- ³V. G. Dubrovskii, G. E. Cirlin, I. P. Soshnikov, A. A. Tonkikh, N. V. Sibirev, Yu. B. Samsonenko, and V. M. Ustinov, *Phys. Rev. B* **71**, 205325 (2005).
- ⁴M. T. Björk, B. J. Ohlsson, T. Sass, A. I. Persson, C. Thelander, M. H. Magnusson, K. Deppert, L. R. Wallenberg, and L. Samuelson, *Nano Lett.* **2**, 87 (2002).
- ⁵S. Gradecak, F. Qian, Y. Li, H. G. Park, and C. M. Lieber, *Appl. Phys. Lett.* **87**, 173111 (2005).
- ⁶A. B. Greytak, L. J. Lauhon, M. S. Gudiksen, and C. M. Lieber, *Appl. Phys. Lett.* **84**, 4176 (2004).
- ⁷T. Bryllert, L. E. Wernersson, T. Lowgren, and L. Samuelson, *Nanotechnology* **17**, S227 (2006).
- ⁸P. J. Pauzauskie and P. Yang, *Mater. Today* **9**, 36 (2006).
- ⁹O. Hayden, G. F. Zheng, P. Agarwal, and C. M. Lieber, *Small* **3**, 2048 (2007).
- ¹⁰R. S. Wagner and W. C. Ellis, *Appl. Phys. Lett.* **4**, 89 (1964).
- ¹¹S. K. Chan, Y. Cai, N. Wang, and I. K. Sou, *J. Cryst. Growth* **301-302**, 866 (2007).
- ¹²J. C. Harmand, M. Tchernycheva, G. Patriarche, L. Travers, F. Glas, and G. Cirlin, *J. Cryst. Growth* **301-302**, 853 (2007).
- ¹³M. Tchernycheva, L. Travers, G. Patriarche, J. C. Harmand, G. E. Cirlin, and V. G. Dubrovskii, *J. Appl. Phys.* **102**, 094313 (2007).
- ¹⁴K. A. Dick, K. Deppert, T. Martensson, S. Mandl, L. Samuelson, and W. Seifert, *Nano Lett.* **5**, 761 (2005).
- ¹⁵A. I. Persson, L. E. Froberg, S. Jeppesen, M. T. Bjork, and L. Samuelson, *J. Appl. Phys.* **101**, 034313 (2007).
- ¹⁶A. Zangwill, *Physics at Surfaces* (Cambridge University Press, Cambridge, 1988).
- ¹⁷V. G. Dubrovskii and N. V. Sibirev, *Phys. Rev. E* **70**, 031604 (2004).
- ¹⁸D. Kashchiev, *Cryst. Growth Des.* **6**, 1154 (2006).
- ¹⁹F. Glas, J. C. Harmand, and G. Patriarche, *Phys. Rev. Lett.* **99**, 146101 (2007).
- ²⁰V. G. Dubrovskii, N. V. Sibirev, R. A. Suris, G. E. Cirlin, J. C. Harmand, and V. M. Ustinov, *Surf. Sci.* **601**, 4395 (2007).
- ²¹A. I. Persson, M. W. Larsson, S. Stengstrom, B. J. Ohlsson, L. Samuelson, and L. R. Wallenberg, *Nature Mater.* **3**, 678 (2004).
- ²²P. Mohan, J. Motohisa, and T. Fukui, *Nanotechnology* **16**, 2903 (2005).
- ²³A. Fontcuberta i Morral, J. Arbiol, J. D. Prades, A. Cirera, and J. R. Morante, *Adv. Mater. (Weinheim, Ger.)* **19**, 1347 (2007).
- ²⁴R. Leitsmann and F. Bechstedt, *J. Appl. Phys.* **102**, 063528 (2007).
- ²⁵T. Akiyama, K. Sano, K. Nakamura, and T. Ito, *Jpn. J. Appl. Phys., Part 2* **45**, L275 (2006).
- ²⁶T. Akiyama, K. Nakamura, and T. Ito, *Phys. Rev. B* **73**, 235308 (2006).
- ²⁷V. G. Dubrovskii and N. V. Sibirev, *Phys. Rev. B* **77**, 035414 (2008).
- ²⁸J. C. Harmand, G. Patriarche, N. Péré-Laperne, M.-N. Mérat-Combes, L. Travers, and F. Glas, *Appl. Phys. Lett.* **87**, 203101 (2005).
- ²⁹E. I. Givargizov, *Highly Anisotropic Crystals* (Springer, Berlin, 1987).
- ³⁰W. Seifert, M. Borgstrom, K. Deppert, K. A. Dick, J. Johansson, M. W. Larsson, T. Martensson, N. Skold, C. P. T. Svensson, B. A. Wacaser, L. R. Wallenberg, and L. Samuelson, *J. Cryst. Growth* **272**, 211 (2004).
- ³¹V. G. Dubrovskii, I. P. Soshnikov, N. V. Sibirev, G. E. Cirlin, and V. M. Ustinov, *J. Cryst. Growth* **289**, 31 (2006).
- ³²S. A. Kukushkin and A. V. Osipov, *Prog. Surf. Sci.* **51**, 1 (1996).
- ³³V. G. Dubrovskii and G. E. Cirlin, *Semiconductors* **39**, 1267 (2005).
- ³⁴*Group IV Elements, IV-IV and III-V Compounds*, Landolt-Börnstein, New Series, Group III, Vol. 41, Pt. A, edited by U. Rössler (Springer, Berlin, 2006).
- ³⁵L. D. Landau and E. M. Lifshits, *Statistical Physics* (Butterworth, Washington, DC, 1980), Pt. 1.
- ³⁶V. G. Dubrovskii, N. V. Sibirev, R. A. Suris, G. E. Cirlin, V. M. Ustinov, M. Tchernycheva, and J. C. Harmand, *Semiconductors* **40**, 1103 (2006).
- ³⁷J. Johansson, C. P. T. Svensson, T. Mårtensson, L. Samuelson, and W. Seifert, *J. Phys. Chem. B* **109**, 13567 (2005).
- ³⁸V. G. Dubrovskii and N. V. Sibirev, *J. Cryst. Growth* **304**, 504 (2007).
- ³⁹D. Kashchiev, *Nucleation: Basic Theory with Applications* (Butterworth Heinemann, Oxford, 2000).
- ⁴⁰C.-Y. Yeh, Z. W. Lu, S. Froyen, and A. Zunger, *Phys. Rev. B* **46**, 10086 (1992).
- ⁴¹J. Johansson, L. S. Karlsson, C. P. T. Svensson, T. Mårtensson, B. A. Wacaser, K. Deppert, L. Samuelson, and W. Seifert, *Nature Mater.* **5**, 574 (2006).
- ⁴²D. J. Eaglesham, A. E. White, L. C. Feldman, N. Moriya, and D. C. Jacobson, *Phys. Rev. Lett.* **70**, 1643 (1993).
- ⁴³A. A. Stekolnikov and F. Bechstedt, *Phys. Rev. B* **72**, 125326 (2005).
- ⁴⁴F. M. Ross, J. Tersoff, and M. C. Reuter, *Phys. Rev. Lett.* **95**, 146104 (2005).